9

Wood Physics/Mechanical Properties

Tao Shi, Haoyuan Liu, Fengze Sun, Jianyi Zhu, Hui Peng, Jianxiong Lyu and Tianyi Zhan*

Stabilization of hygro-deformation and interaction between earlywood and latewood in Chinese fir

https://doi.org/10.1515/hf-2025-0054 Received April 26, 2025; accepted August 22, 2025; published online September 5, 2025

Abstract: The alternating arrangement of earlywood (EW) and latewood (LW) in wood growth reflects an optimization structure, where anatomical differences lead to varying properties. This study analyzed the stabilization characteristics of hygro-deformation in Chinese fir, and compared the dimensional responses of intact growth rings and with those of isolated EW and LW during step-wise desorption and adsorption. During both desorption and adsorption, both LW and EW exhibited rapid hygro-deformation initially, followed by stabilization. The stabilization of dimensional changes lagged behind stabilization of moisture content based on evaluating their rates of change. Isolated EW showed significant reductions in hygro-deformation compared to when LW was present, due to the removal of LW's restraining effect. The radial and tangential shrinking differences in EW before and after isolation were 0.40 and 0.46 %, respectively, as relative humidity decreased from 97 % to 0. The corresponding values were 0.58 and 0.71 % during adsorption (0 \rightarrow 97 % RH). These results highlight the impact of EW-LW interaction on the hygro-deformation of Chinese fir and are helpful to elucidate the complex nature of wood-water relations.

Keywords: growth ring; isolation; digital image correlation (DIC); shrinking and swelling; restraining effect

1 Introduction

In regions with distinct seasonal changes, trees develop wood in annual growth increments, forming recognizable growth rings. These rings reflect the tree's growth throughout different seasons. In softwoods, there are significant structural differences between earlywood (EW) and latewood (LW) (Siau 2012). EW forms at the beginning of the growing season under favorable conditions, featuring larger, thinner-walled cells that enhance water transport and nutrient flow. In contrast, LW develops towards the end of the growing season when growth slows, characterized by smaller, thicker-walled cells that provide the wood's overall strength and structural stability. The alternating arrangement of EW and LW across growth rings represents an iterative optimization process for adaptive growth (Eder et al. 2008; Wei et al. 2024).

Both EW and LW cells consist of cellulose, hemicellulose, and lignin. Cellulose provides the fundamental structural, hemicellulose supports cell wall flexibility, and lignin contributes rigidity to the cell wall. These components are hygroscopic to varying degrees, i.e., they absorb or release moisture depending on the ambient environment. This moisture exchange causes the wood to swell or shrink during moisture adsorption or desorption. Understanding the hygro-deformation (swelling and shrinking) of EW and LW is crucial for managing the dimensional stability of wood (Krzemień et al. 2015; Pang et al. 1999; Perré and Huber 2007).

Key structural factors affecting the hygro-deformation include density and microfibril angle (MFA) (Kollmann and Cote Jr 1968; Siau 2012). Denser woods tend to deform more than less dense one. Higher MFA, such as in juvenile wood (Garcia et al. 2022) or compression wood (Zhan et al. 2021), leads to greater longitudinal and less transverse shrinking. The variations in the hygro-deformation along the radial and tangential directions wood has been attributed to arrangement of EW and LW, presence of ray cells, differences in the cell composition along the parallel and perpendicular direction of the S₂ cell wall layer, difference of MFA in radial and tangential walls, as well as the influence of the middle

^{*}Corresponding author: Tianyi Zhan, Co-Innovation Center of Efficient Processing and Utilization of Forest Resources, College of Materials Science and Engineering, Nanjing Forestry University, Nanjing 210037, China, E-mail: tyzhan@njfu.edu.cn. https://orcid.org/0000-0002-2120-6062

Tao Shi, Haoyuan Liu, Fengze Sun, Jianyi Zhu, Hui Peng and Jianxiong Lyu, Co-Innovation Center of Efficient Processing and Utilization of Forest Resources, College of Materials Science and Engineering, Nanjing Forestry University, Nanjing 210037, China

lamella (Arzola-Villegas et al. 2019; Ross 2010; Skaar 2012). It is widely reported that, at certain moisture content (MC) changes, LW generally exhibits more significant hygrodeformation than EW (Garcia et al. 2022; Lanvermann et al. 2014: Liu et al. 2023: Yin et al. 2023). EW and LW shrink and swell at different rates, resulting in anisotropic hygrodeformation, particularly along radial and tangential directions. In the radial direction, EW and LW are arranged in series, while in the tangential direction, they are arranged parallel, with LW dominating movement and forcing EW to deform more significantly (Ma and Rudolph 2006; Ouyang et al. 2022). Consequently, dimensional variations are larger in the tangential direction (5-10%) compared to the radial direction (2-6%) (Garcia et al. 2020a). This differential shrinking contributes to crack and impacts wood drying quality (Fu et al. 2023).

Research on hygro-deformation of EW or LW is typically conducted at the tissue (Fu et al. 2021; Patera et al. 2018; Redman et al. 2016), cell (Joffre et al. 2016; Rafsanjani et al. 2014; Yin et al. 2023) and cell wall levels (Gao et al. 2024; Larsson et al. 2024; Li et al. 2024; Paajanen et al. 2022). While some studies focus on EW and LW separately (Almeida et al. 2014; Patera et al. 2013; Perré and Huber 2007), other examines EW and LW behaviors when both are present (Lanvermann et al. 2014, Patera et al. 2018, Zhan et al. 2023). It is reported that the strain concentrations occur along the EW-LW interface (Krzemień et al. 2015), with large hygrodeformation of EW due to the restraining effect of LW. In the previous study (Zhan et al. 2023), digital image correlation (DIC) technique was employed to capture the intra-ring

variation of hygro-deformation from EW and LW, and to qualitatively observe the restraining effect exerted by adjacent LW from the previous growth ring on EW. However, the quantitative evaluation of this restraining effect has not yet been reported. The present study served as a follow-up to Zhan et al. (2023). First, the stabilization durations of both dimensional and MC within the growth ring were analyzed to determine whether they stabilize simultaneously. Subsequently, EW and LW regions were physically isolated, and their hygro-deformation was re-measured. Finally, the restraining effect was quantitatively assessed by comparing hygro-deformation before and after isolation.

2 Materials and methods

2.1 Materials

Three samples of air-dried Chinese fir wood (*Cunninghamia lanceolata* [Lamb.] Hook.) were obtained with dimensions of 5 mm \times 3 mm \times 0.5 mm (radial \times tangential \times longitudinal, R \times T \times L), each containing the intact 17th growth ring. These samples were water-saturated and polished with a cryomicrotome HM 560 (Microm, Germany) removing 2- μ m thin transverse slices, and were then fully equilibrated over distilled water for over 4 weeks. Following sorption and hygro-deformation experiments, the samples were mechanically divided into isolated EW (\sim 4 \times 3 \times 0.5 mm³, R \times T \times L) and LW (\sim 0.5 \times 3 \times 0.5 mm³, R \times T \times L) regions. Figure 1 illustrates the detailed sampling procedure, a

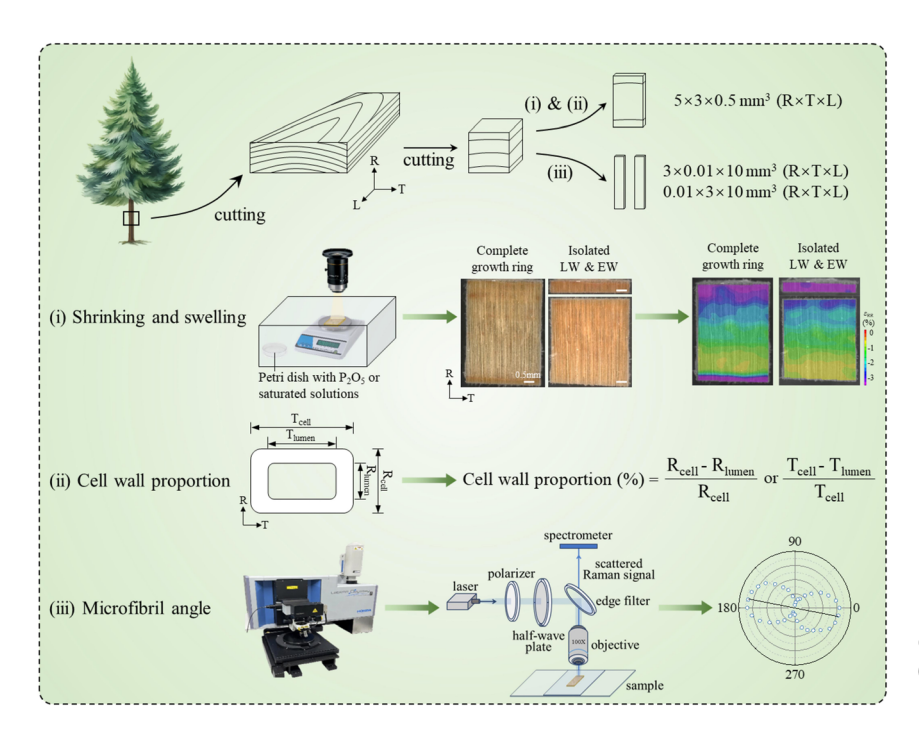


Figure 1: Sampling procedure and three major characterizations: (i) shrinking and swelling, (ii) cell wall proportion, and (iii) microfibril angle.

typical sample with the intact growth ring and the isolated EW and LW regions were shown in step (i) for hygrodeformation and cell wall proportion experiments (step ii). Additionally, sections measuring $3 \times 0.01 \times 10 \text{ mm}^3 (R \times T \times L)$ and $0.01 \times 3 \times 10 \text{ mm}^3$ (R × T × L) were also cut from both EW and LW regions for step (iii) - MFA determination. The average air-dried density of the samples was approximately 370 kg/m^3 .

2.2 Sorption and hygro-deformation experiment

Before conducting the hygro-deformation tests, the surface evenness of the samples was assessed using a digital microscope (VHX-7000, Keyence Company, Japan) to ensure they were free of warping, thereby avoiding any interference with subsequent in-plane deformation measurements. The desorption, adsorption and corresponding shrinking and swelling experiments followed the methodology outlined by Zhan et al. (2023). Successively, the intact growth ring samples and isolated LW and EW samples underwent the desorption and adsorption processes. Relative humidity (RH) levels of 97, 75, 58, 33, or 0 % were maintained using saturated salt solution (K₂SO₄, NaCl, MgCl₂ or NaBr) or P₂O₅ in a sealed container. An electronic analytical balance (Mettler Toledo ME204, \pm 0.1 mg) was placed in the sealed container for measuring mass change, i.e. MC, of the wood sample. At each humidity level, MC values were recorded periodically at 0, 3, 6, 9, 12, 24, 36, 48, 60, 72, 96, 120 and 144 h. Cross-sectional morphology was imaged using the focal length adjusted digital microscope without removing the samples from the sealed container, thereby preventing any MC variation during observation (Figure 1). The microscope was equipped with a 12.22-megapixel complementary metal oxide-semiconductor image sensor, providing a resolution of $6,144 \times 4,608$ pixels. Three samples each of the intact growth ring and isolated LW or EW samples were replicated to determine average MC and hygro-deformation values. A representative sample was selected to display in-plane strain distribution.

The hygro-deformation was assessed using DIC analysis (VIC-2D software, Correlated Solution Inc., United States), with the following steps (Garcia et al. 2020a, b; Zhan et al. 2023): (i) selecting the area of interest (AOI): approximately $15 \,\mathrm{mm}^2$ (2,567 \times 3,679 pixels²) for the intact growth ring sample; (ii) dividing the AOI into evenly spaced virtual grids (subsets: 113), step size selection (28) and predefining the correlation criterion, interpolation, thresholding and postprocessing to calculate the full-field strain; and (iii) extracting strain data from 2D contour plot through lines across the

growth ring. The strains in the $X(\varepsilon_{TT})$ and $Y(\varepsilon_{RR})$ directions represented tangential and radial deformations, respectively. Shrinking or swelling strain was determined by comparing images of the equilibrated sample at 97 or 0 % RH as a reference, following the definition used for wood shrinking or swelling (Peng et al. 2012). Shrinking strain was treated as negative and swelling strain as positive to depict dimensional changes during moisture desorption and adsorption.

2.3 Hygro-deformation difference between isolated and intact LW/EW

The hygro-deformation differences were calculated as follows:

$$\Delta \varepsilon_{RR-EW} = \varepsilon_{RR-grEW} - \varepsilon_{RR-iEW}$$
 (1)

$$\Delta \varepsilon_{\text{TT-EW}} = \varepsilon_{\text{TT-grEW}} - \varepsilon_{\text{TT-EW}}$$
 (2)

$$\Delta \varepsilon_{\text{RR-LW}} = \varepsilon_{\text{RR-iLW}} - \varepsilon_{\text{RR-grLW}}$$
 (3)

$$\Delta \varepsilon_{\text{TT-LW}} = \varepsilon_{\text{TT-iLW}} - \varepsilon_{\text{TT-grLW}}$$
 (4)

where $\Delta \varepsilon_{RR}$ and $\Delta \varepsilon_{TT}$ represent the radial and tangential hygro-deformation differences, respectively. The subscripts "gr" and "i" denote measurements taken from samples within the intact growth ring and after isolation, respectively. Specifically, the hygro-deformation differences were evaluated for both the desorption process from 97 % RH to 0 and the adsorption process from 0 to 97 % RH.

2.4 Cell wall proportion

After hygro-deformation experiments, the isolated EW and LW were placed in an environmental scanning electron microscope (FEI Quanta FEG 600, FEI Company, USA) for determination of cell wall proportion. The cross-section images of EW and LW were obtained at an acceleration voltage of 4 kV in a low-vacuum mode. The cell wall proportion was quantified by calculating the ratio of cell wall thickness to cell thickness for both radial and tangential directions separately (Figure 1, step ii). For each direction, measurements were taken from 20 cells in either EW or LW to ensure replicability.

2.5 MFA

The 10-µm-thick section was mounted on a glass slide with a drop of deionized water, and the coverslip was sealed with

nail polish to prevent water evaporation. MFA determination employed polarized confocal Raman microscopy (Xplora HR Evolution, Horiba Jobin Yvon, Japan) following the methods by Gierlinger et al. (2009) and Zhang et al. (2023). The imaging employed a 100× oil immersion lens (NA 1.40) and a 532 nm laser with 100 % intensity. A 600 mm grating was used with a wavenumber range of 100–3,900 cm⁻¹ and an integration time of 20 s. Raman spectra were obtained by rotating a half-wave plate in 5° increments to vary laser polarization, capturing measurements at 10° interval across a full 360° polarization range to analyze Raman intensity as a function of polarization angle. MFAs on both the tangential and radials wall were evaluated with five replicates each in EW and LW.

2.6 Statistical analysis

The statistical software, SPSS version 17.0 (SPSS Inc, Chicago, IL, USA) was used for data analysis. Significant effects of sampling location (EW or LW) and RH level on hygrodeformation (difference) stress were analyzed by Duncan's multiple comparison test (p = 0.05).

3 Results and discussion

3.1 Hygro-deformation during desorption and adsorption

The hygro-deformation behavior of Chinese fir during desorption (Figures 2 and 3) and adsorption (Figures 4 and 5) is presented. Figures 2 and 4 display the full-field distributions of radial strains (ε_{RR}), while Figures 3 and 5 show tangential strains (ε_{TT}). In Figures 2b, 3b, 4b, and b5b, the evolution of strain over time is shown alongside the corresponding changes in MC. MC represents the average value for the intact growth ring sample, with the sampling locations for LW, EW and restrained EW indicated in the bottomright subfigure of Figure 2a. Previous studies (Patera et al. 2018; Zhan et al. 2023) attributed the larger hygrodeformation of restrained EW at the growth ring interface to the mechanical restraint imposed by the previous LW on EW. Throughout both the desorption and adsorption processes, LW consistently exhibited greater dimensional changes compared to both restrained EW and unrestrained EW, regardless of humidity levels. Specifically, when comparing dimensions at 97 % RH to those at RH of 0 after desorption, the values of ε_{RR} and ε_{TT} for LW were -3.0 % and -4.2 %, respectively, while the corresponding values for EW were -1.1 % and -3.3 %. After fully adsorption from RH of 0 back to 97 %, ε_{RR} reached 2.82 % for LW and 1.04 % for EW, while ε_{TT} values were 3.64 % and 2.78 %, respectively.

Notably, these values were lower than those reported for Chinese fir in the literature (Cheng 1985: Jiang and Lu 2012; Yao et al. 2017), as well as for other coniferous species with comparable densities (Perré and Huber 2007; Thybring and Fredriksson 2023; Watanabe et al. 1998). The variation in hygro-deformation of wood was closely related to density and MFA, and also influenced by the content of lignin and hydrophilic extractives (Eder et al. 2020; Jankowska et al. 2017). In addition, the origin of hygro-deformation variability should also consider structural differences within the wood; even two trees of the same species can exhibit significant differences in EW shrinking (Almeida et al. 2014). In terms of anisotropy, LW show a lower $\varepsilon_{\rm TT}/\varepsilon_{\rm RR}$ ratio (1.4) than EW (3.0) when RH decreased from 97 % to 0, indicating that EW was more anisotropic. Both ratios were higher than those reported in the literature, where LW is generally considered to be nearly isotropic (Patera et al. 2018; Perré and Huber 2007).

The dimensional changes after full stabilization as a function of difference of MC (Δ MC) are shown in Figure 6. It could be found that the dimensional changes exhibited a quasi-linear relationship with Δ MC, regardless of anatomical tissue type or direction. Notably, the radial deformation (ε_{RR}) (Figure 6a and c) differed significantly between LW and (restrained) EW, whereas the differences in tangential deformation (ε_{TT}) were relatively minor (Figure 6b and d). This reduction variation in ε_{TT} may be attributed to the dominant influence of LW, which constrained the tangential deformation of adjacent EW, resulting in a more uniform overall response across the growth ring (Ouyang et al. 2022).

3.2 Stabilization of hygro-deformation and MC

Based on the results in Figures 2–5, it was observed that $\varepsilon_{\rm RR}$ and $\varepsilon_{\rm TT}$, along with MC, changed rapidly at the start of the desorption or adsorption before stabilizing, expectedly. However, the stabilized periods differed between dimensional changes and MC. To precisely evaluate the stabilizations of dimension and MC, the variations of dimension and MC with logarithmic time were plotted in Figures 7–10. Taken desorption at 0 humidity as an example, MC tended to be constant after 48 h (indicated as the purple arrows, bottom subfigure in Figures 7g and 8g), whereas $\varepsilon_{\rm RR}$ and $\varepsilon_{\rm TT}$ stabilized after 108 h (black arrows in Figures 7g and 8g), similar results could be seen during adsorption (Figures 9 and 10). The desorption or adsorption process involved not only sorption equilibrium but also a time-dependent

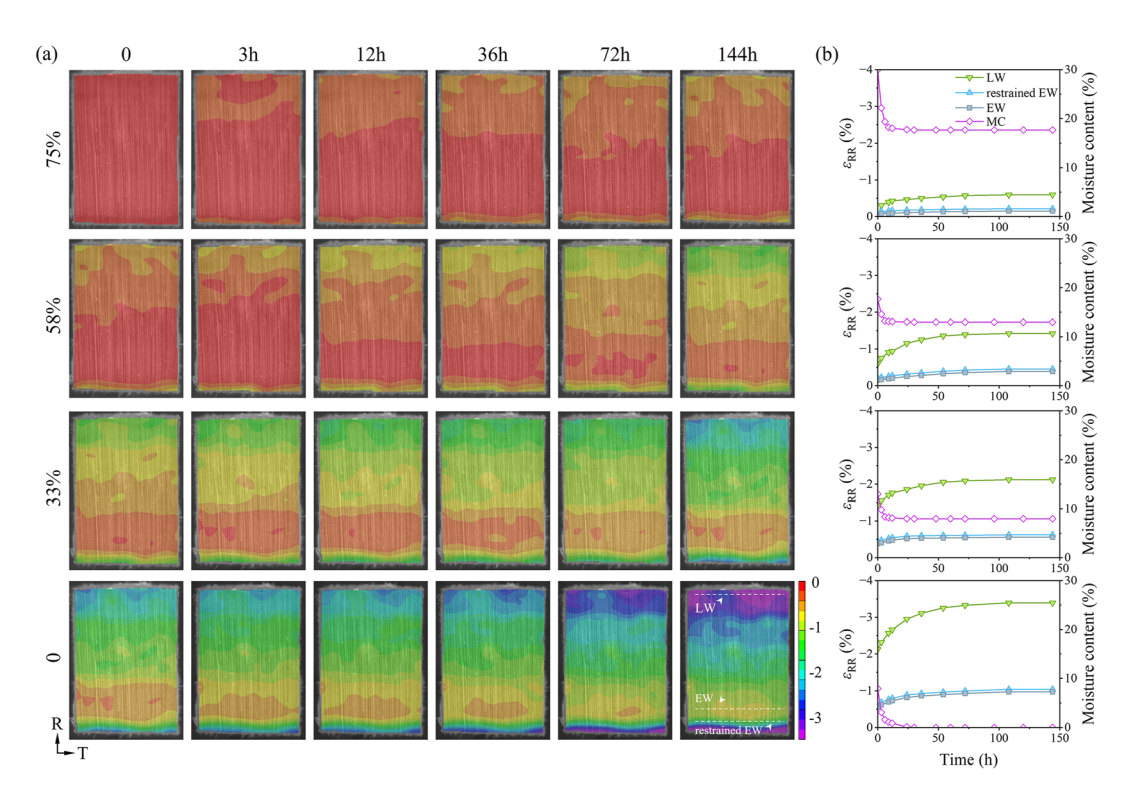


Figure 2: Changes in shrinking in radial direction (ε_{RR}) with stepwise RH decrements (97 % \rightarrow 75 % \rightarrow 58 % \rightarrow 33 % \rightarrow 0): full-field distribution of ε_{RR} (a) and its time-dependent value along with MC variation (b). The values of ε_{RR} shown in (b) were averaged from the sampling positions indicated in the bottom-right subfigure of (a). Full-field distributions of ε_{RR} in (a) after 144 h desorption were cited from Zhan et al. (2023).

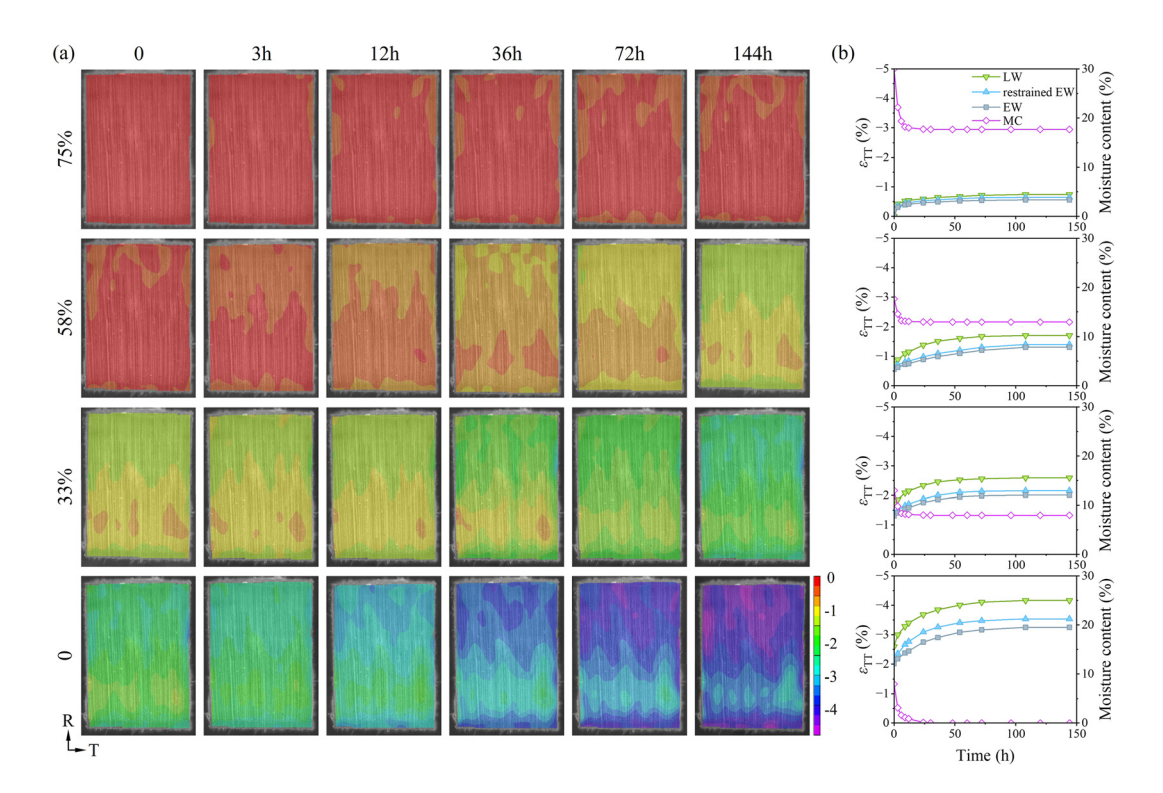


Figure 3: Changes in shrinking in tangential direction (ε_{TT}) with stepwise RH decrements (97 % \rightarrow 75 % \rightarrow 58 % \rightarrow 33 % \rightarrow 0): full-field distribution of ε_{TT} (a) and its time-dependent value along with MC variation (b). Sampling positions in (b), refer to Figure 2. Full-field distributions of ε_{TT} in (a) after 144 h desorption were cited from Zhan et al. (2023).

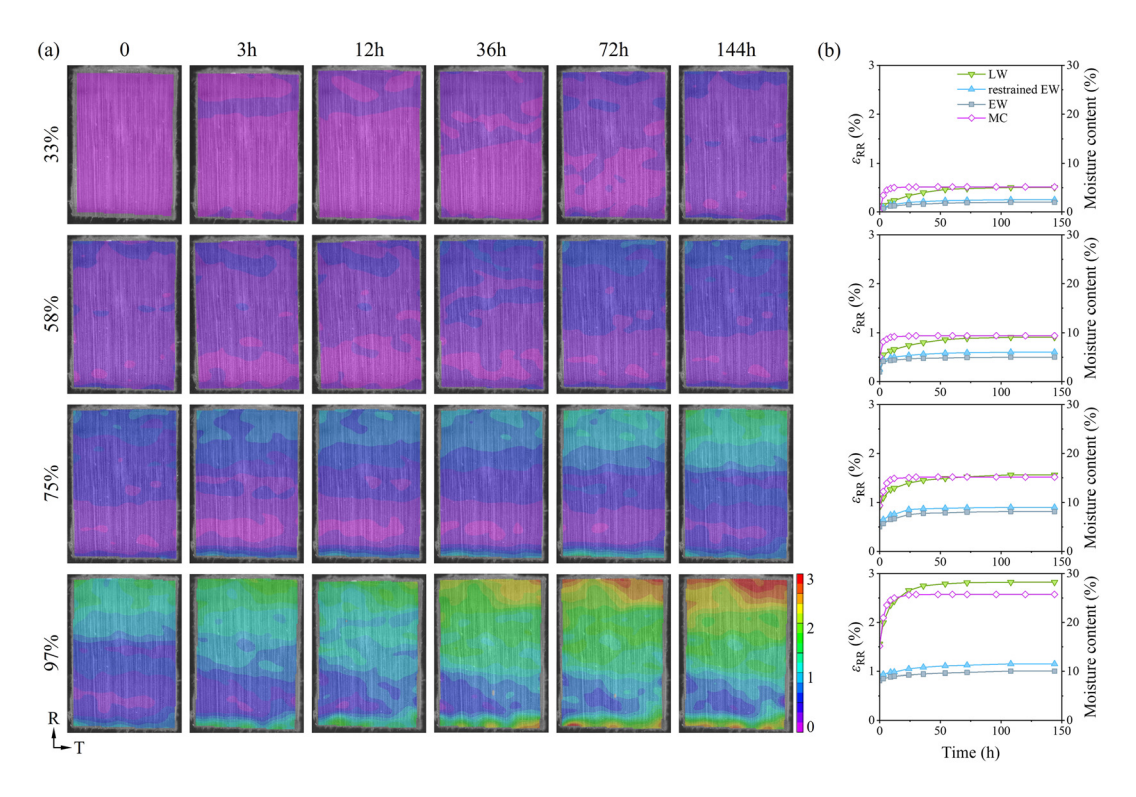


Figure 4: Changes in swelling in radial direction (ε_{RR}) with stepwise RH increments (0 \rightarrow 33 % \rightarrow 58 % \rightarrow 75 % \rightarrow 97 %): full-field distribution of ε_{RR} (a) and its time-dependent value along with MC variation (b). Sampling positions and arrows in (b), refer to Figure 2. Full-field distributions of ε_{RR} in (a) after 144 h adsorption were cited from Zhan et al. (2023).

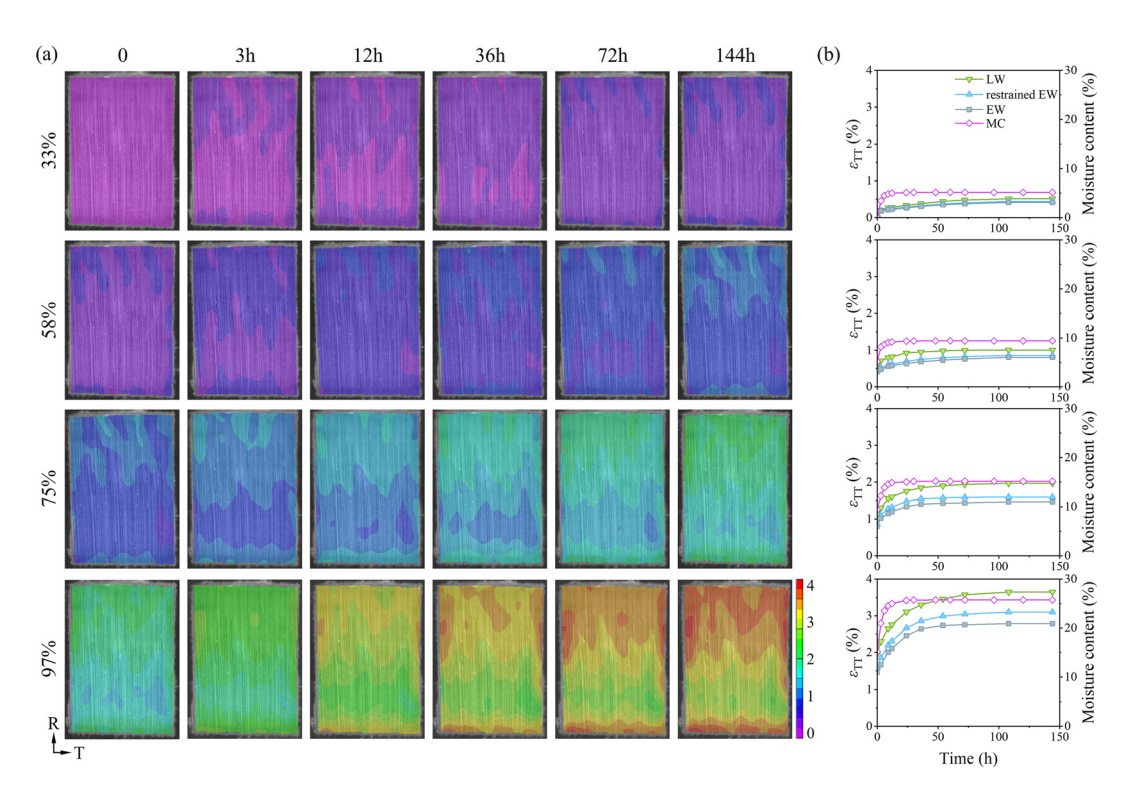


Figure 5: Changes in swelling in tangential direction (ϵ_{TT}) with stepwise RH increments ($0 \rightarrow 33 \% \rightarrow 58 \% \rightarrow 75 \% \rightarrow 97 \%$): full-field distribution of ϵ_{TT} (a) and its time-dependent value along with MC variation (b). Sampling positions in (b), refer to Figure 2. Full-field distributions of ϵ_{TT} in (a) after 144 h adsorption were cited from Zhan et al. (2023).

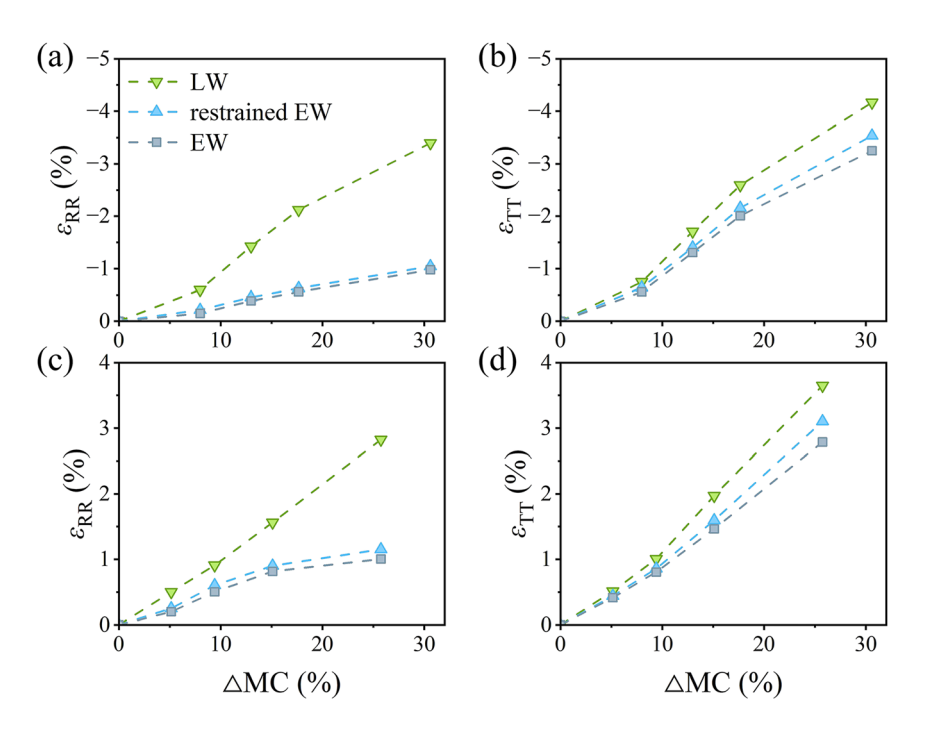


Figure 6: Relationships between strain ε_{RR} (a, c) and ε_{TT} (b, d) and difference of MC (Δ MC) during desorption (a, b) and adsorption (c, d) processes.

macromolecular relaxation of the wood polymers. As water molecules were absorbed, hemicelluloses and other amorphous polymers within the cell wall softened and transitioned toward a rubbery state. This softening facilitated stress relaxation, enabling internal polymer conformation, which contributed to a delayed dimensional response even when MC remained constant (Brémaud and Gril 2021: Hunt and Gril 1996; Uehara et al. 2025). Consequently, shrinking or swelling did not perfectly track changes in MC; instead, the internal polymer relaxation led to hysteresis and a time lag in dimensional adjustment.

In this study, MC and strains were not monitored continuously, but rather measured at several specific time points. Therefore, the exact time required for stabilization among MC and strains could not be determined. Nevertheless, the available results allowed for a comparative analysis of the differences in the stabilization behavior between MC and strains. These delayed stabilization of ϵ_{RR} and ϵ_{TT} relative to MC contrasts with findings from the literature (Ma et al. 2010; Nopens et al. 2019; Ouyang et al. 2022). Ouyang et al. (2022) observed that the size of Catalpa bungei samples stabilized immediately once MC reached equilibrium, using real-time dynamic vapor sorption combined with a digital microscope. Besides, Ma et al. (2010) reported that the dimensional change of Picea sitchensis Carr. occurred more rapidly than MC change. However, the stabilization periods

of dimension and MC reported in this study were not comparable with published literature due to variations in environmental conditions. Since maintaining constant humidity was challenging when temperature fluctuated, various methods were used to control RH, such as saturated salt solutions in this study, and humidity generators in the reported literature. Besides, this non-simultaneous behavior could be associated with variations in sample size and the characterization of length scales as well. The sample size used in this study $(5 \times 3 \times 0.5 \text{ mm}^3, R \times T \times L)$ was smaller than those reported in the literature: $20 \times 20 \times 1.5 \text{ mm}^3 (R \times T \times L)$ (Nopens et al. 2019), and $20 \times 20 \times 4 \text{ mm}^3$ (R × T × L) (Ma et al. 2010). When examined sample sizes across multiple growth rings, the observed length scale was typically restricted to the macro scale. Ouyang et al. (2022) reported using samples of $8 \times 4 \times 4$ mm³ (R × T × L), but measured dimensional change across a series of cells from one vessel to another. According to Rafsanjani et al. (2014), the hygro-deformation of wood cell wall was substantially larger than the one of wood tissues with the growth ring and wood samples made of several growth rings, because the interactions between cell wall layers, cell wall and middle lamella, and between cells contributed to deformation at the cell wall and cellular scales (Zhan et al. 2023). Benefiting from the full-field hygrodeformation provided by DIC, the analysis in this study was able to focus on the dimensional changes within a few cells.

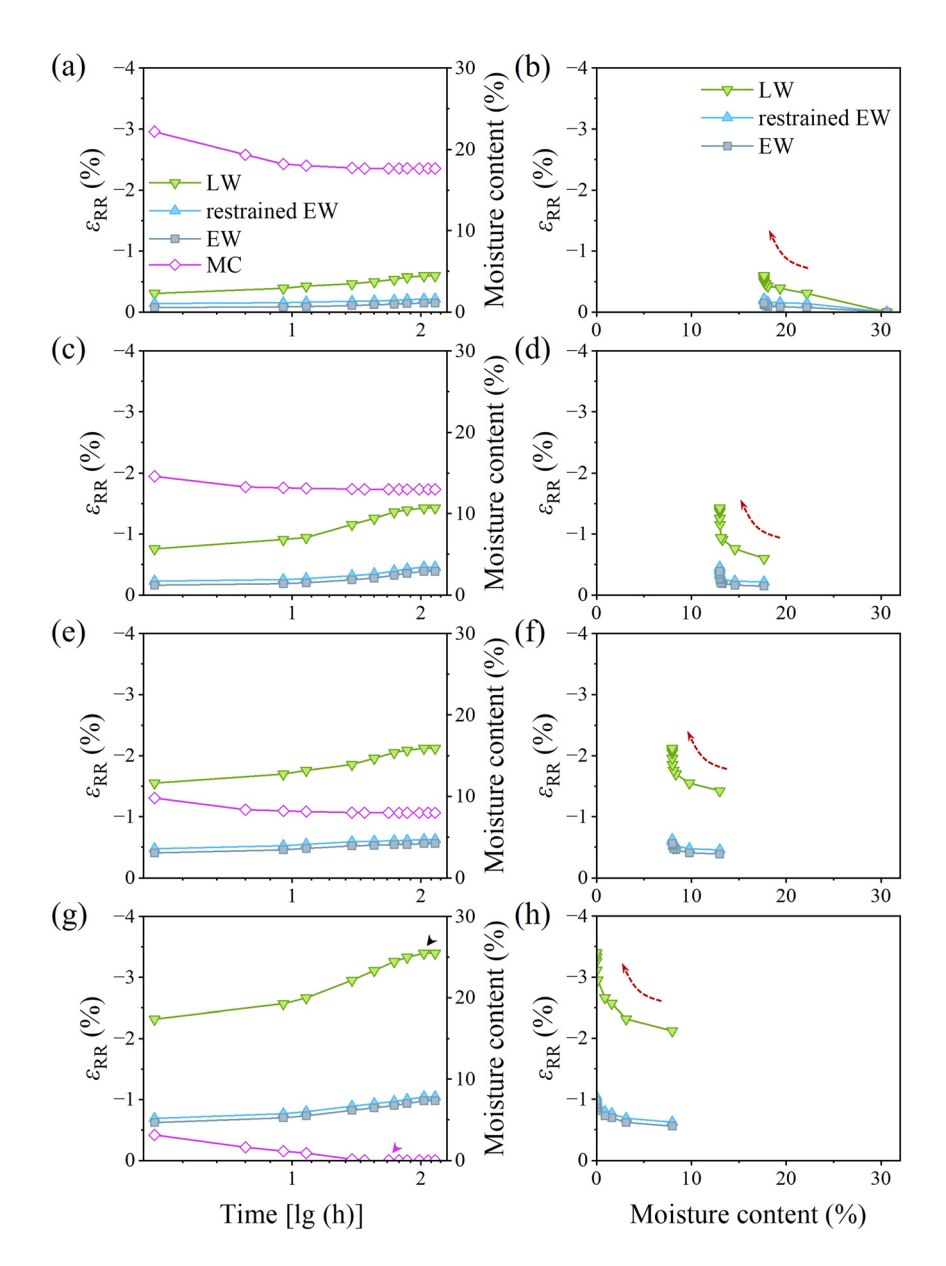


Figure 7: MC and ε_{RR} as a function of logarithmic desorption time (a, c, e, g), and corresponding evolutions of ε_{RR} versus MC (b, d, f, h). RH level: 75 % (a, b), 58 % (c, d), 33 % (e, f) and 0 (g, h). The purple and black arrows in (g) indicated the stabilized duration of MC and dimension, respectively.

The relationships between strains and MC during desorption (right side of Figures 7 and 8) and adsorption (right side of Figures 9 and 10) were constructed. In these figures, the strain exhibited a trend of initially rapid and then slower change with decreasing (or increasing) MC. On the one hand, the desorption (or adsorption) of water molecules from (or onto) the polar groups of wood components directly caused changes in cell wall dimensions, corresponding to the initial rapid phase of strain variation with MC. Additionally, the hygro-deformation of wood was influenced by the state of moisture as well. During sorption

process, moisture gradually returned to its equilibration state. This equilibration dependent on interaction with the chemical constituents of the wood cell wall (Nakano 1994). As moisture equilibrated, changes in the size and quantity of nanopores within the wood cell wall occurred (Shi and Avramidis 2019), potentially causing slight dimensional deformations. To assess the impact of moisture state on dimensional changes, it was recommended to record real-time variations in MC and dimensions using dynamic vapor sorption and high-resolution microscopy. Additionally, further investigations could be performed to understand

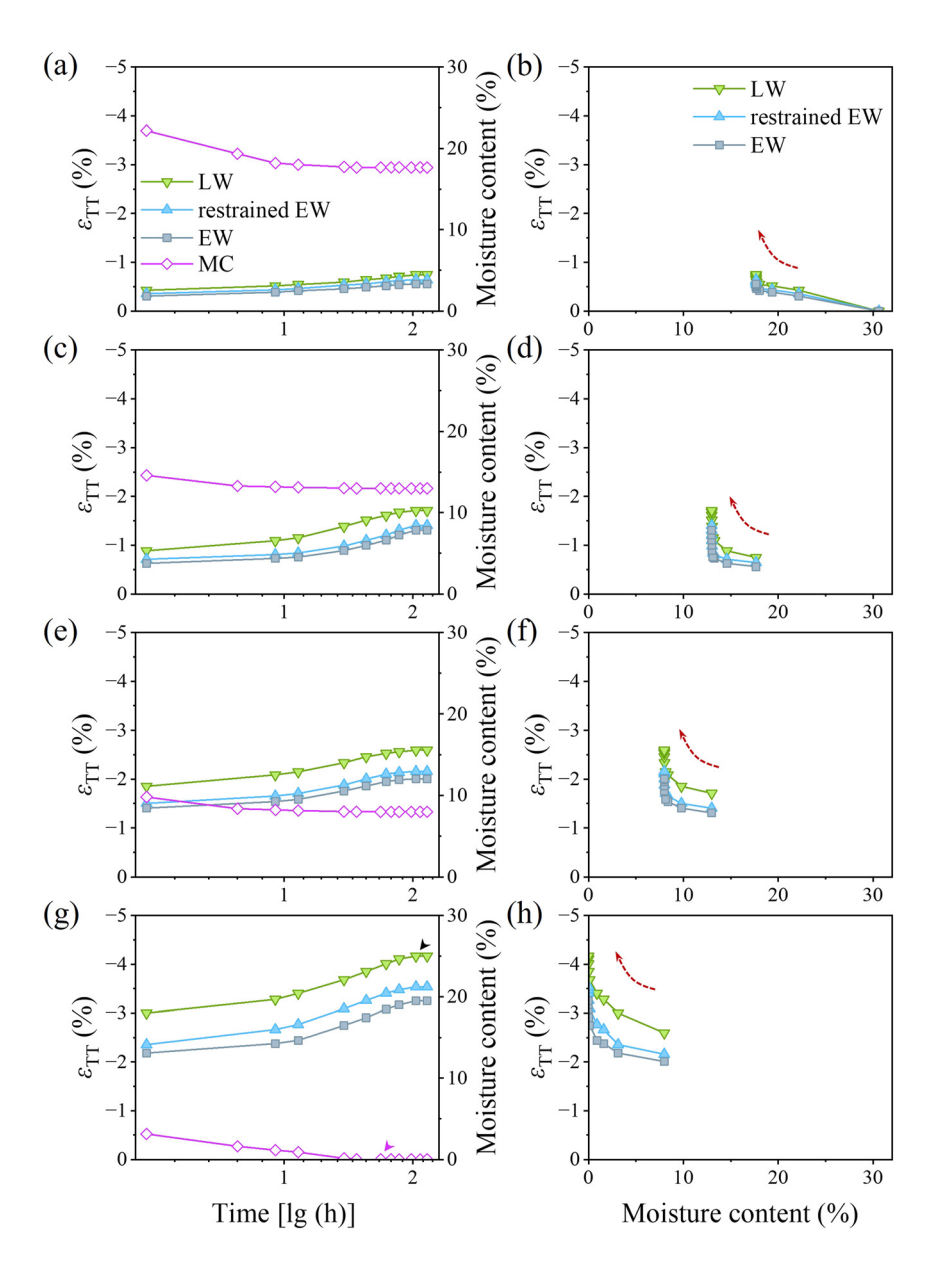


Figure 8: MC and ε_{TT} as a function of logarithmic desorption time (a, c, e, g), and corresponding evolutions of ε_{TT} versus MC (b, d, f, h). RH level: 75 % (a, b), 58 % (c, d), 33 % (e, f) and 0 (g, h). The purple and black arrows in (g), refer to Figure 7.

how RH levels affect the stabilization of dimensions, as the relationship between RH and moisture presence remained unclear (Li and Ma 2022; Telkki et al. 2013).

3.3 Hygro-deformation difference between isolated and intact LW/EW

The full-field hygro-deformation was compared between the intact growth ring samples and isolated LW and EW samples. Figure 11 shows the comparison of the shrinking results. When the intact growth ring sample was divided as two parts as well as LW from the last growth ring was removed, the restraining effect disappeared, specifically leading to reductions in shrinking in EW. These reductions were characterized as $\Delta \varepsilon_{RR}$ (Figure 11c) and $\Delta \varepsilon_{TT}$ (Figure 11d). Besides, there were also reductions of ε_{RR} and ε_{TT} in transition wood (TW) from the isolated samples compared to that within the intact growth ring samples. However, no significant variation in ε_{RR} or ε_{TT} was found between isolated LW and LW within the intact growth ring.

Figure 12 displays the swelling results. Similarly, obvious reductions of ε_{RR} (a) and ε_{TT} were observed in EW and TW in the isolated samples. These reductions demonstrated that LW

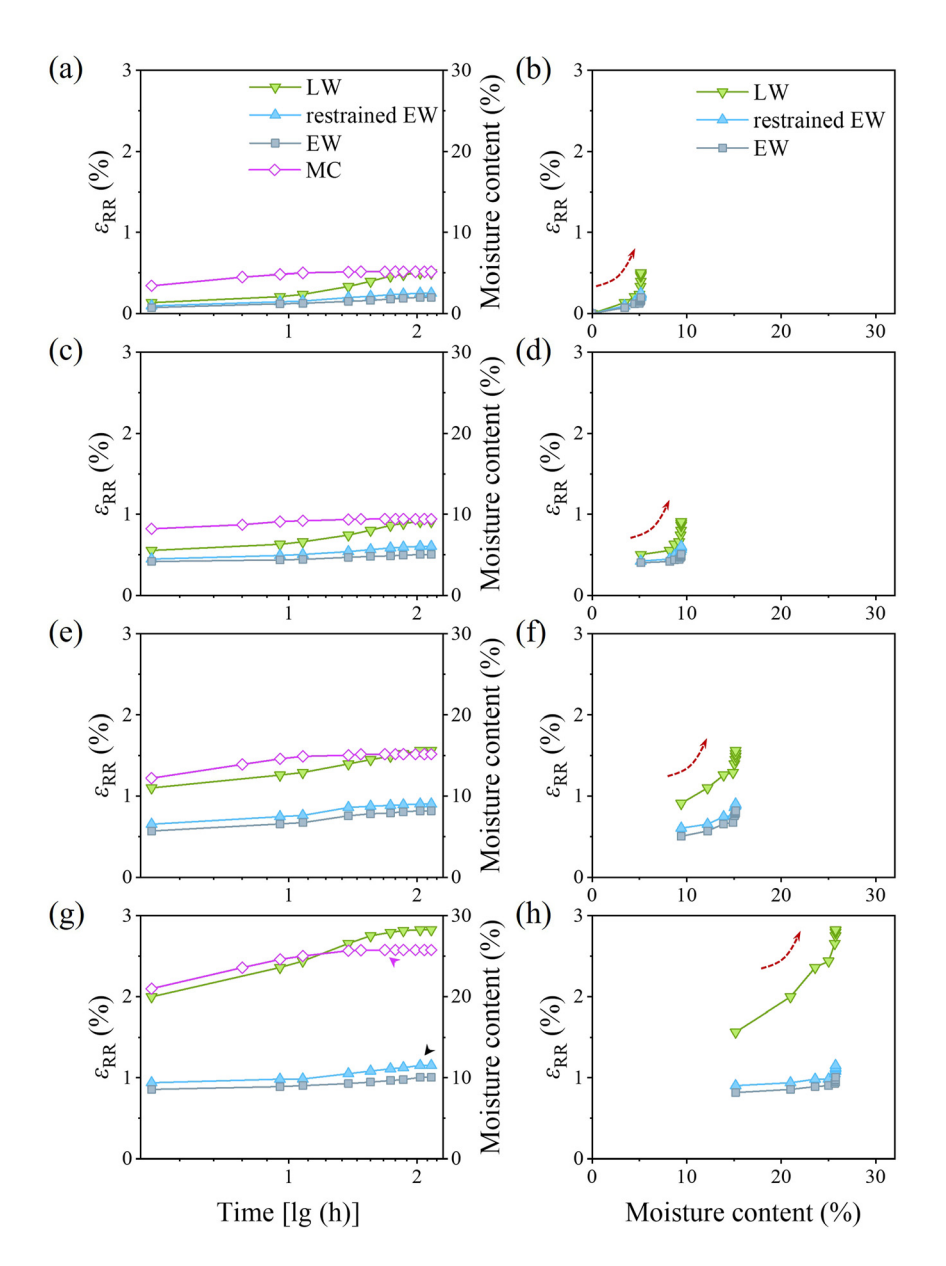


Figure 9: MC and ε_{RR} as a function of logarithmic adsorption time (a, c, e, g), and corresponding evolutions of ε_{RR} versus MC (b, d, f, h). RH level: 33 % (a, b), 58 % (c, d), 75 % (e, f) and 97 % (g, h). The purple and black arrows in (g), refer to Figure 7.

promoted hygro-deformation in both adjacent EW and TW. LW had higher stiffness and more hygro-deformation than EW and TW. In hence, EW and TW were forced to deform with LW during sorption process, attributing to higher hygro-deformation of EW and TW within the intact growth ring. The value of $\Delta \varepsilon_{\rm TT}$ was higher than $\Delta \varepsilon_{\rm RR}$, regardless of shrinking (Figure 11c and 11d) or swelling (Figure 12c and 12d). During desorption, the values of $\Delta \varepsilon_{\rm TT}$ and $\Delta \varepsilon_{\rm RR}$ were 0.46 and 0.40 %, respectively. The corresponding values were 0.58 and 0.71 % during adsorption. The variations in $\Delta \varepsilon_{\rm TT}$ and $\Delta \varepsilon_{\rm RR}$ were influenced by the interaction between EW and LW. This interaction originated from the structural variation.

Particularly, MFA and cell wall thickness are key determinants of wood's stiffness and hygro-deformation (Eder et al. 2020). Figure 13 provides a detailed overview of the variations in MFA and cell wall proportion in both radial and tangential walls between EW and LW. It was evident that EW exhibited higher MFAs and lower cell wall proportions compared to LW, irrespective of the wall orientation. The greater values of $\Delta \varepsilon_{\rm TT}$ compared to $\Delta \varepsilon_{\rm RR}$ could be explained by the more pronounced difference in MFA within the tangential wall. Specifically, LW had the lowest MFA in the tangential wall (7.6°), while its cell wall proportion (18.3 %) was lower than that in radial wall (22.2 %). It should be noted that the cell

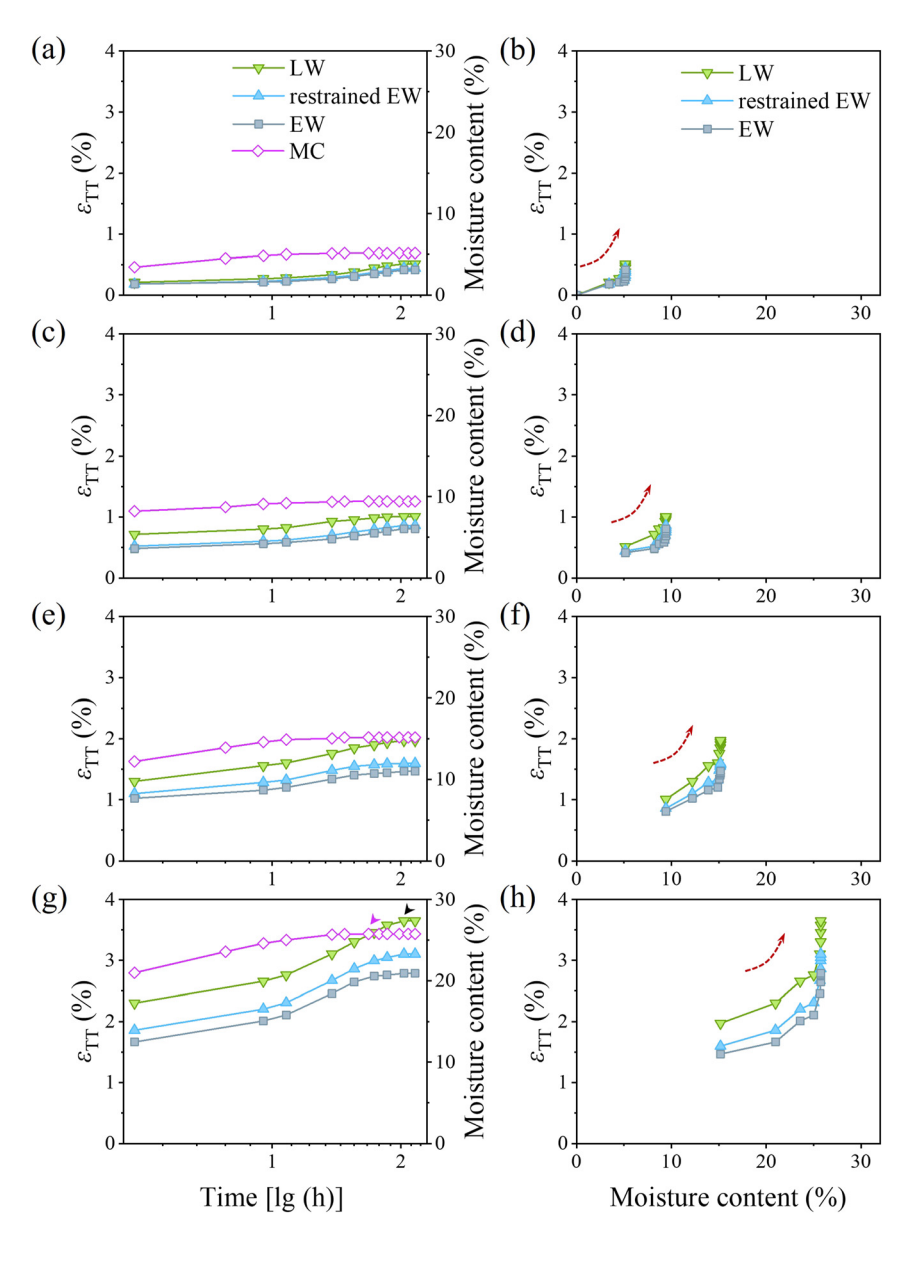


Figure 10: MC and $\varepsilon_{\rm TT}$ as a function of logarithmic adsorption time (a, c, e, g), and corresponding evolutions of ε_{TT} versus MC (b, d, f, h). RH level: 33 % (a, b), 58 % (c, d), 75 % (e, f) and 97 % (g, h). The purple and black arrows in (g), refer to Figure 7.

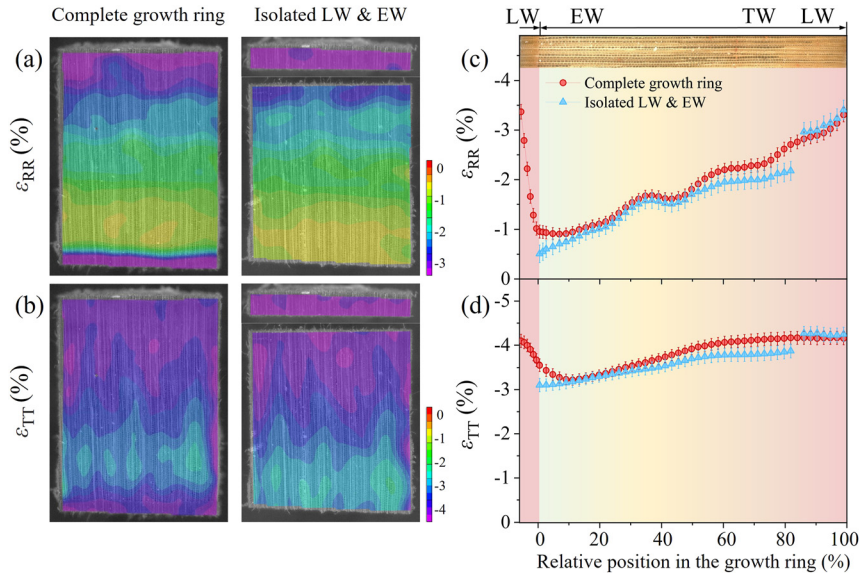


Figure 11: Comparison of shrinking results in intact growth ring samples and isolated EW and LW samples when RH changed from 97 %to 0: full-field distribution of ε_{RR} (a) and ε_{TT} (b), and corresponding relationships between shrinking strain and relative position in the growth ring (c and d). The results obtained from the intact growth ring samples were referenced from Zhan et al. (2023).

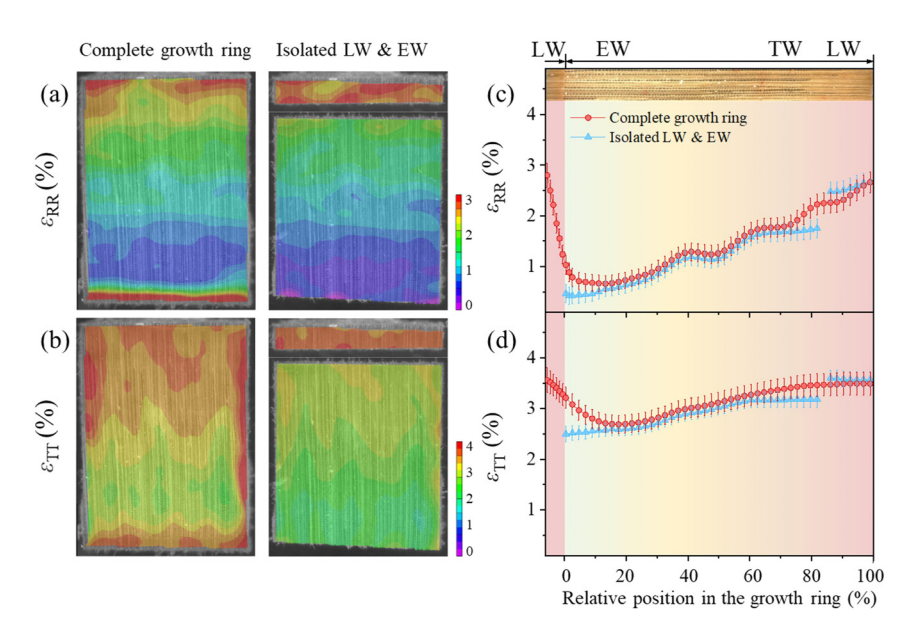


Figure 12: Comparison of swelling results in intact growth ring samples and isolated EW and LW samples when RH changed from 0 to 97 %: full-field distribution of ε_{RR} (a) and ε_{TT} (b), and corresponding relationships between swelling strain and relative position in the growth ring (c and d). The results obtained from the intact growth ring samples were referenced from Zhan et al. (2023).

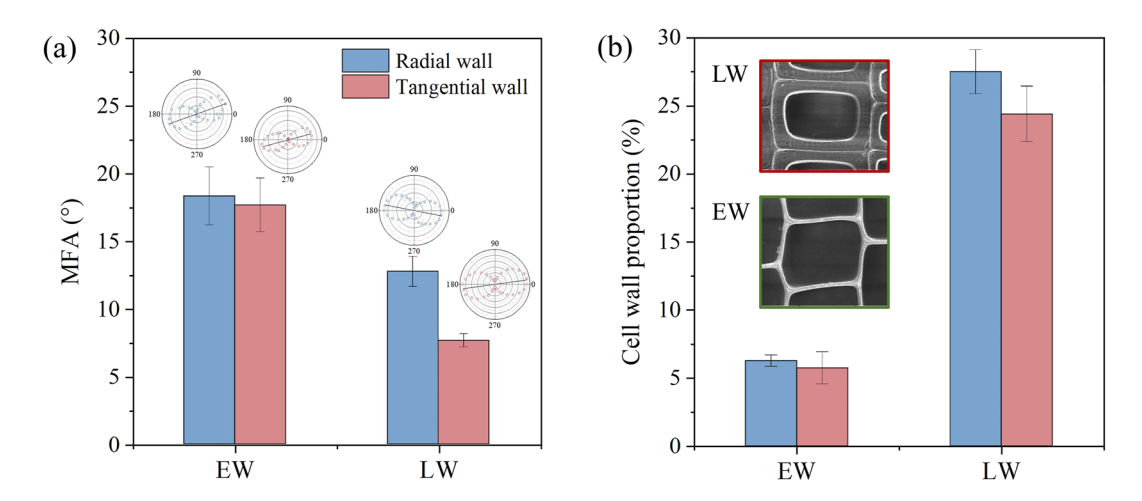


Figure 13: Variations of MFA (a) and cell wall proportion (b) of EW and LW in radial and tangential walls. Polar plots in (a) illustrated the intensity variations of the 1,096 cm⁻¹ Raman band as the polarization direction of the incident laser was rotated in 10° steps. Inset in (b) presented the SEM images of LW and EW. Scale bars: 10 μm.

wall proportion in this study was lower than that reported in a previous study (Zhan et al. 2021) using the same species, as it was calculated based on a line ratio (Figure 1) rather than an area ratio.

Comparing the difference of strain in intact growth ring and isolated EW and LW is helpful to understand the interaction between EW and LW, and probably to assess the evolution of moisture variation induced stresses. When the interaction stress exceeds transverse tensile strength, the likelihood of cracking in the wood increases significantly (Qu et al. 2025). Future research could further evaluate the elastic

and even viscoelastic stresses under varying hygro-thermal conditions which simulate practical drying environments.

4 Conclusions

During both desorption and adsorption, LW and (restrained) EW exhibited rapid hygro-deformation initially, followed by stabilization. This stabilization in dimensional changes (ε_{RR} and ε_{TT}) lagged behind that observed in MC. Although no significant variation in shrinking or swelling was detected in

isolated LW compared to that within the intact growth ring, isolated EW samples demonstrated notable reductions of shrinking and swelling due to the removal of LW's restraining effect. The hygro-deformation differences in EW before and after isolation were quantified. When RH decreased from 97 % RH to 0, the differences were 0.40 and 0.46 % in radial and tangential directions, respectively. The corresponding values were 0.58 and 0.71 % during adsorption (0 \rightarrow 97 % RH). The strain differences could be potentially used to evaluate the possibility for wood cracking. These results highlight the impact of EW-LW interaction on the hygro-deformation of Chinese fir and are helpful to elucidate the complex nature of wood-water relations.

Research ethics: Not applicable. **Informed consent:** Not applicable.

Author contributions: The authors have accepted responsibility for the entire content of this manuscript and approved its submission.

Use of Large Language Models, AI and Machine Learning

Tools: None declared.

Conflict of interest: The authors state no conflict of interest. **Research funding:** This work was financially supported by the National Natural Science Foundation of China (No. 32171705).

Data availability: The raw data can be obtained on request from the corresponding author.

References

- Almeida, G., Huber, F., and Perre, P. (2014). Free shrinkage of wood determined at the cellular level using an environmental scanning electron microscope. Maderas-Cienc. Tecnol. 16: 187-198.
- Arzola-Villegas, X., Lakes, R., Plaza, N.Z., and Jakes, J.E. (2019). Wood moistureinduced swelling at the cellular scale - Ab Intra. Forests 10: 996.
- Brémaud, I. and Gril, J. (2021). Moisture content dependence of anisotropic vibrational properties of wood at quasi equilibrium: analytical review and multi-trajectories experiments. Holzforschung 75: 313-327.
- Cheng, J. (1985). Wood science. China Forestry Pub, Beijing.
- Eder, M., Jungnikl, K., and Burgert, I. (2008). A close-up view of wood structure and properties across a growth ring of Norway spruce (Picea abies [L] Karst.). Trees 23: 79-84.
- Eder, M., Schäffner, W., Burgert, I., and Fratzl, P. (2020). Wood and the activity of dead tissue. Adv. Mater. 33: 2001412.
- Fu, Z., Chen, J., Zhang, Y., Xie, F., and Lu, Y. (2023). Review on wood deformation and cracking during moisture loss. *Polymers* 15: 3295.
- Fu, Z., Weng, X., Gao, Y., and Zhou, Y. (2021). Full-field tracking and analysis of shrinkage strain during moisture content loss in wood. Holzforschung 75: 436-443.
- Gao, Y., Fu, Z., Fu, F., Zhou, Y., Gao, X., and Zhou, F. (2024). Mechanism of wood deformation cascading from nanoscale to macroscale in response to moisture desorption. Cellulose 31: 6581-6595.

- Garcia, R.A., Rosero-Alvarado, J., and Hernández, R.E. (2020a). Full-field moisture-induced strains of the different tissues of tamarack and red oak woods assessed by 3D digital image correlation. Wood Sci. Technol. 54: 139-159.
- Garcia, R.A., Rosero-Alvarado, J., and Hernández, R.E. (2020b). Swelling strain assessment of fiber and parenchyma tissues in the tropical hardwood Ormosia coccinea. Wood Sci. Technol. 54: 1447-1461.
- Garcia, R.A., Rosero-Alvarado, J., and Hernández, R.E. (2022). Moistureinduced strains in earlywood and latewood of mature and juvenile woods in jack pine from 3D-DIC measurements. Wood Mater. Sci. Eng.
- Gierlinger, N., Luss, S., König, C., Konnerth, J., Eder, M., and Fratzl, P. (2009). Cellulose microfibril orientation of Picea abies and its variability at the micron-level determined by Raman imaging. J. Exp. Bot. 61: 587-595.
- Hunt, D.G. and Gril, J. (1996). Evidence of a physical ageing phenomenon in wood. J. Mater. Sci. Lett. 15: 80-82.
- Jankowska, A., Drożdżek, M., Sarnowski, P., and Horodeński, J. (2017). Effect of extractives on the equilibrium moisture content and shrinkage of selected tropical wood species. BioResources 12: 597-607.
- Jiang, J. and Lu, J. (2012). Shrinkage-swelling properties of dried Chinese fir woods. J. Central South Univ. For. Technol. 32: 152-157.
- Joffre, T., Isaksson, P., Dumont, P.J.J., Roscoat, S.R.d., Sticko, S., Orgéas, L., and Gamstedt, E.K. (2016). A method to measure moisture induced swelling properties of a single wood cell. Exp. Mech. 56: 723-733.
- Kollmann, F. and Cote, Jr, W. (1968). Principles of wood science and technology. I: solid wood. Springer-Verlag, New York.
- Krzemień, L., Strojecki, M., Wroński, S., Tarasiuk, J., and Łukomski, M. (2015). Dynamic response of earlywood and latewood within annual growth ring structure of Scots pine subjected to changing relative humidity. Holzforschung 69: 555-561.
- Lanvermann, C., Wittel, F.K., and Niemz, P. (2014). Full-field moisture induced deformation in Norway spruce: intra-ring variation of transverse swelling. Eur. J. Wood Wood Prod. 72: 43-52.
- Larsson, P.T., Alfthan, J., Simeonova, G., and Holmgvist, C. (2024). Changes in the macro and nano-structure of paper during moisture cycling. Cellulose 31: 2743-2764.
- Li, J. and Ma, E. (2022). 2D time-domain nuclear magnetic resonance (2D TD-NMR) characterization of cell wall water of Fagus sylvatica and Pinus taeda L. Cellulose 29: 8491-8508.
- Li, J., Pan, C., and Ma, E. (2024). Cell wall water induced dimensional changes of beech and pine wood. Ind. Crop Prod. 214: 118544.
- Liu, J., Liu, W., Tan, R., Huang, W., Wang, B., Zhang, S., and Zhang, M. (2023). Drying strain behavior of elm earlywood and latewood with digital image correlation method. Dry. Technol. 41: 746-753.
- Ma, E., Nakao, T., Zhao, G., Ohata, H., and Kawamura, S. (2010). Relation between moisture sorption and hygroexpansion of sitka spruce during adsorption processes. Wood Fiber Sci. 42: 304-309.
- Ma, Q. and Rudolph, V. (2006). Dimensional change behavior of Caribbean pine using an environmental scanning electron microscope. Dry. Technol. 24: 1397-1403.
- Nakano, T. (1994). Non-steady state water adsorption of wood. Wood Sci. Technol. 28: 359-363.
- Nopens, M., Riegler, M., Hansmann, C., and Krause, A. (2019). Simultaneous change of wood mass and dimension caused by moisture dynamics. Sci. Rep. 9: 10309.
- Ouyang, B., Yin, F., Li, Z., and Jiang, J. (2022). Study on the moisture-induced swelling/shrinkage and hysteresis of Catalpa bungei wood across the growth ring. Holzforschung 76: 711-721.

- Paajanen, A., Zitting, A., Rautkari, L., Ketoja, J.A., and Penttilä, P.A. (2022). Nanoscale mechanism of moisture-induced swelling in wood microfibril bundles. *Nano Lett.* 22: 5143–5150.
- Pang, S., Orchard, R., and McConchie, D. (1999). Tangential shrinkage of Pinus radiata earlywood and latewood, and its implication for withinring internal checking. N. Z. J. For. Sci. 29: 484–491.
- Patera, A., Derome, D., Griffa, M., and Carmeliet, J. (2013). Hysteresis in swelling and in sorption of wood tissue. *J. Struct. Biol.* 182: 226–234.
- Patera, A., Van den Bulcke, J., Boone, M.N., Derome, D., and Carmeliet, J. (2018). Swelling interactions of earlywood and latewood across a growth ring: global and local deformations. *Wood Sci. Technol.* 52: 91–114.
- Peng, M., Ho, Y.-C., Wang, W.-C., Cui, Y.-H., and Gong, M. (2012). Measurement of wood shrinkage in jack pine using three dimensional digital image correlation (DIC). *Holzforschung* 66: 639–643.
- Perré, P. and Huber, F. (2007). Measurement of free shrinkage at the tissue level using an optical microscope with an immersion objective: results obtained for Douglas fir (*Pseudotsuga menziesii*) and spruce (*Picea abies*). *Ann. For. Sci.* 64: 255–265.
- Qu, J., Gong, Y., Li, M., and Ren, H. (2025). Evolution of interlaminar shear failure in CLT: insights from theoretical calculation, acoustic emission, and microstructural analysis. *Constr. Build. Mater.* 470: 140510.
- Rafsanjani, A., Stiefel, M., Jefimovs, K., Mokso, R., Derome, D., and Carmeliet, J. (2014). Hygroscopic swelling and shrinkage of latewood cell wall micropillars reveal ultrastructural anisotropy. J. R. Soc., Interface 11: 20140126.
- Redman, A.L., Bailleres, H., Turner, I., and Perré, P. (2016). Characterisation of wood–water relationships and transverse anatomy and their relationship to drying degrade. Wood Sci. Technol. 50: 739–757.
- Ross, R.J. (2010). Wood handbook: wood as an engineering material. General Technical Report FPL-GTR-190. USDA Forest Service, Forest Products Laboratory, Madison, p. 509, 1 v. 190.
- Shi, J. and Avramidis, S. (2019). Evolution of wood cell wall nanopore size distribution in the hygroscopic range. Holzforschung 73: 899–910.
 Siau, J.F. (2012). Transport processes in wood. Springer, Berlin/New York.
 Skaar, C. (2012). Wood-water relations. Springer, Berlin/New York.

- Telkki, V.-V., Yliniemi, M., and Jokisaari, J. (2013). Moisture in softwoods: fiber saturation point, hydroxyl site content, and the amount of micropores as determined from NMR relaxation time distributions. *Holzforschung* 67: 291–300.
- Thybring, E.E. and Fredriksson, M. (2023). Wood and moisture. In: Niemz, P., Teischinger, A., and Sandberg, D. (Eds.). Springer handbook of wood science and technology. Springer International Publishing, Cham, pp. 355–397.
- Uehara, K., Horiyama, H., Miyoshi, Y., Yamashita, K., Kojiro, K., and Furuta, Y. (2025). Mechanism of changes in the mechanical properties of wood due to water adsorption and desorption described by rheological considerations. *Holzforschung* 79: 328–339.
- Watanabe, U., Fujita, M., and Norimoto, M. (1998). Transverse shrinkage of coniferous wood cells examined using replica method and power spectrum analysis. *Holzforschung* 52: 200–206.
- Wei, Y., Zheng, C., Ma, L., Jiang, X., Yin, Y., and Guo, J. (2024). Inter- and intragrowth ring variations of wood carbon fractions in *Pinus tabuliformis*. *Holzforschung* 78: 137–147.
- Yao, M., Yang, Y., Song, J., Yu, Y., and Jin, Y. (2017). Lignin-based catalysts for Chinese fir furfurylation to improve dimensional stability and mechanical properties. *Ind. Crop. Prod.* 107: 38–44.
- Yin, F., Jiang, J., Sheng, S., Wang, P., Yang, Y., and Yin, Y. (2023). Properties of Catalpa bungei (Bignoniaceae) earlywood and latewood in the same growth ring during moisture adsorption/desorption: swelling and shrinkage at the cell level. IAWA J. 45: 195–212.
- Zhan, T., Lyu, J., and Eder, M. (2021). In situ observation of shrinking and swelling of normal and compression Chinese fir wood at the tissue, cell and cell wall level. *Wood Sci. Technol.* 55: 1359–1377.
- Zhan, T., Liu, H., Zhu, J., Sun, F., Peng, H., and Lyu, J. (2023). A close-up view of the intra-ring variation of transverse shrinking and swelling in Chinese fir using digital image correlation without artificial speckle pattern. *Wood Sci. Technol.* 57: 1369–1383.
- Zhang, X., Li, L., and Xu, F. (2023). Polarized Raman spectroscopy for determining the orientation of cellulose microfibrils in wood cell wall. *Cellulose* 30: 75–85.